Synthesis, Electrochemistry, and Structural Studies of Lithium Intercalation of a Nanocrystalline Li_2MnO_3-like Compound

Gaurav Jain,[†] Jingsi Yang,[†] Mahalingam Balasubramanian,[‡] and Jun John Xu*[,†]

Materials Science and Engineering, Rutgers, The State University of New Jersey, Piscataway, New Jersey 08854, and Experimental Facilities Division, Sector 20, Advanced Photon Source, Argonne National Laboratory, Argonne, Illinois 60439

Received February 15, 2005. Revised Manuscript Received June 3, 2005

A nanocrystalline lithium-rich manganese (IV) oxide, synthesized by a low-temperature sol−gel route, is reported as a surprising lithium intercalation host. The composition of the material is very close to Li_2MnO_3. X-ray diffraction (XRD), electron diffraction, and high-resolution transmission electron microscopy analyses establish that the material possesses a nanocrystalline structure, similar to that of the rock salt monoclinic Li_2MnO_3, with a crystallite size of about 5 nm. X-ray absorption spectroscopy (XAS) analysis at the Mn K edge indicates that the Mn is in the 4+ oxidation state and in a local atomic/electronic environment similar to that in the rock salt monoclinic Li_2MnO_3. Unlike the microcrystalline Li_2MnO_3, which is known to be electrochemically inactive for lithium intercalation or deintercalation, this nanocrystalline counterpart surprisingly yields a reversible intercalation capacity of 0.71−0.87 Li per formula or 163−200 (mA h)/g and a specific energy density of 400−450 (mW h)/g, at different current rates, with excellent capacity retention over repeated cycling. In situ XAS analysis, conducted during discharge and charge, shows the occurrence of highly reversible Faradaic processes, with reduction and oxidation of Mn. Electrochemical data, namely, low hysteresis in the charge/discharge voltage profiles, excellent cycling performance, and the charge coefficient being constantly at unity, in conjunction with structural data, namely, XAS and XRD collected during/after electrochemical tests showing that the material retains its original structure, establish the excellent electrochemical and structural stability and reversibility of the compound. The role of nanocrystallinity, lack of long-range order, defects, disorder, and nanostructured morphology are discussed to relate to the surprising intercalation properties of this nanocrystalline compound.

Introduction

Rechargeable lithium batteries, with first-row transition-metal compounds as cathodes and lithium or carbon-based anodes, are most attractive in terms of energy density, battery life, and reliability. The cathodes in these batteries work on the principle of reversible intercalation and deintercalation of lithium ions into/from the transition-metal compound host structure.[1−4] Typically, the cathode compounds are transition-metal oxides that have close-packed oxygen arrays, which provide a framework structure and specific sites for topotactic insertion and removal of lithium ions. Among numerous transition-metal oxides, manganese oxide based compounds are particularly attractive as cathodes for their lower cost and nontoxicity.[5] The spinel $LiMn_2O_4$ has emerged as one of the promising candidates with a capacity of 120 (mA h)/g at 4 V versus Li.[6−8] However, various capacity fade problems associated with this compound of Mn in the 3.5+ oxidation state have been identified.[8,9] Numerous researchers have emphasized the importance of developing substituted manganese oxides with oxidation state of Mn greater than 3.5+, as cathode materials with better cycling stability.[8−11]

In the Li−Mn−O phase diagram, there are a series of compounds lying along the tie line from the defect-spinel λ-MnO_2 to the rock salt Li_2MnO_3 with Mn in the 4+ oxidation state.[5] These compounds possess cubic close packing of oxygen with varying configurations of Mn and Li occupying different octahedral and/or tetrahedral sites. At one end of this tie line, the λ-MnO_2, with a defect spinel structure,[12] is known to allow substantial lithium intercalation.[13] The spinel $Li_4Mn_5O_{12}$[14−18] and the defect spinel $Li_2Mn_4O_9$[14,19] are prominent lithium-rich phases along this

* To whom correspondence should be addressed. Phone: (732) 445 5606. Fax: (732) 445 3258. E-mail: johnxu@rci.rutgers.edu.
[†] The State University of New Jersey.
[‡] Argonne National Laboratory.

(1) Whittingham, M. S. *Science* **1976**, *192*, 1126.
(2) Goodenough, J. B. *Solid State Ionics* **1994**, *69*, 184.
(3) Ohzuku, T.; Ueda, A. *Solid State Ionics* **1994**, *69*, 201.
(4) Thackeray, M. M.; Thomas, J. O.; Whittingham, M. S. *MRS Bull.* **2000**, *25*, 29.
(5) Thackeray, M. M. *Prog. Solid State Chem.* **1997**, *25*, 1.
(6) Thackeray, M. M.; David, W. I. F.; Bruce, P. G.; Goodenough, J. B. *Mater. Res. Bull.* **1983**, *18*, 461.
(7) Tarascon, J. M.; Guyomard, D. *Electrochim. Acta* **1993**, *38*, 9, 1221.
(8) Gummow, R. J.; De Kock, A.; Thackeray, M. M. *Solid State Ionics* **1994**, *69*, 59.
(9) Yang, D. H.; Shin, Y. J.; Oh, S. M. *J. Electrochem. Soc.* **1996**, *143*, 2204.
(10) Amine, K.; Tukamoto, H.; Yasuda, H.; Fujita, Y. *J. Electrochem. Soc.* **1996**, *143*, 1607.
(11) Guohua, L.; Ikuta, H.; Uchida, T.; Wakihara, W. *J. Electrochem. Soc.* **1996**, *143*, 178.
(12) Hunter, J. C. *J. Solid State Chem.* **1981**, *39*, 142.
(13) Mosbah, A.; Verbaere, A.; Tournoux, M. *Mater. Res. Bull.* **1983**, *18*, 1375.
(14) Thackeray, M. M.; De Kock, A.; Rossow, M. H.; Liles, D. C.; Bittihn, R.; Hoge, D. *J. Electrochem. Soc.* **1992**, *139*, 363.

10.1021/cm0503329 CCC: $30.25
Published on Web 06/24/2005

tie line, which have been shown to exhibit promising intercalation properties and good cycling performance. The rock salt Li_2MnO_3, in extreme contrast to these materials, is known to be electrochemically inactive for lithium intercalation or deintercalation.[5,20−23] In the Li_2MnO_3 structure lithium and manganese occupy all the octahedral sites to form a layer of lithium ions and a mixed layer of (1:2) lithium and manganese ions, alternating between close-packed oxygen layers. It has been reported that lithium cannot be conventionally extracted from the Li_2MnO_3, since all the manganese have a valence state of 4+ and cannot be further oxidized.[20,21] At the same time, it is believed that lithium ions cannot be intercalated into the rock salt Li_2MnO_3 structure since all the octahedral sites are fully occupied.[5,22,23] Lithium cannot occupy the vacant tetrahedral sites in such a rock salt structure due to the exceedingly large repulsion from cations in neighboring face-shared octahedral sites.

Despite its inactivity, the rock salt Li_2MnO_3 is of fundamental interest, partly due to the prominence of rock salt structures as lithium intercalation hosts. Commercial lithium ion batteries are based on the rock salt $LiCoO_2$ or its solid solution with the rock salt $LiNiO_2$, which is a promising cathode candidate in its own right and has been extensively investigated.[24−26] The $LiNi_{1/2}Mn_{1/2}O_2$,[21,27−29] $LiNi_{1/3}Co_{1/3}Mn_{1/3}O_2$,[30,31] and related compounds, which have received much attention in the past few years as technologically promising new cathodes, possess rock salt structures as well in which the Mn is in the 4+ valence state and which may be regarded as structurally closely related to the rock salt Li_2MnO_3. For all these compounds, lithium ions are deintercalated out of the rock salt structure first and subsequently intercalated back into the structure in a reversible fashion. However, attempts on insertion of Li into stoichiometric transition-metal compounds with rock salt structures, without deintercalating the lithium ions present in the structures first, so far have not lead to reversible processes. For the rock salt $LiNiO_2$, Dahn et al. showed[32] that, upon discharge versus Li, a phase transformation occurs, leading to formation of a Li_2NiO_2 compound with a 1T-TiS_2 or CdI_2 structure. In this transformation, the cubic close packing of oxygen in the $LiNiO_2$ shears to a hexagonal packing and selected cations from the octahedral sites migrate to tetrahedral sites, allowing lithium intercalation into the tetrahedra neighboring the vacated octahedral sites and forming 1T-Li_2NiO_2. Another form of Li_2NiO_2 with an orthorhombic *Immm* structure synthesized by solid-state reaction was reported by Kang et al.,[33] in which the Li ions also occupy tetrahedral sites, whereas Ni ions are reported to be in square planar sites.[33,34] A Li_2MnO_2 compound with a structure similar to that proposed for the 1T-Li_2NiO_2 was reported to form upon deep discharge of the spinel $LiMn_2O_4$.[35] The phase transformations from a rock salt structure to the 1T-TiS_2 structure are usually exceedingly sluggish and do not occur in all rock salt compounds. Also, the structural changes associated with such a transformation render deintercalation and reversible cycling improbable. Unlike the case of $LiNiO_2$ forming 1T-Li_2NiO_2 upon lithium insertion, efforts to form a $Li_{1+y}CoO_2$ phase have been largely unsuccessful.[32,36] Dahn et al.[32] showed that efforts to insert lithium into rock salt $LiCoO_2$ leads to precipitation of Li_2O and metallic Co clusters, not the formation of a $Li_{1+y}CoO_2$ phase. Alternately, Carewska and co-workers[36] tried solid-state synthesis of $Li_{1+y}CoO_2$, with $y = 0.08, 0.35$. However, they showed that only 10−20% of this intended excess Li resides in the $LiCoO_2$ phase. The sites occupied by the excess Li in this $Li_{1+y}CO_2$ are not exactly understood, though a part of the excess Li incorporated in the material was reported to occupy interstitial sites in the structure.[36]

Considering the inability of Li_2MnO_3 to allow lithium intercalation or deintercalation, various researchers have focused attention on compounds obtained upon Li or Li_2O removal (leaching) from the Li_2MnO_3.[37−39] These studies report high intercalation capacities and good reversibilities for these Li-deficient layered compounds derived from the Li_2MnO_3. Recently, Bruce and co-workers investigated direct electrochemical extraction of lithium from Li_2MnO_3.[21] They reported that this extraction of lithium takes place via non-deintercalation processes of oxygen loss and/or replacement of Li^+ by H^+ in the Li_2MnO_3. West and co-workers recently reported that slight oxygen deficiency of Li_2MnO_3 formed in solid-state synthesis results in a mean Mn oxidation state just slightly lower than 4+, allowing electrochemical extraction of a very small amount of lithium (equivalent to ca. 13 (mA h)/g) from the compound.[40]

(15) Masquelier, C.; Tabuchi, M.; Ado, K.; Kanno, R.; Kobayashi, Y.; Maki, Y.; Nakamura, O.; Goodenough, J. B. *J. Solid State Chem.* **1996**, *123*, 255.
(16) Strobel, P.; Le Cras, F.; Anne, M. *J. Solid State Chem.* **1996**, *124*, 83.
(17) Takada, T.; Hayakawa, H.; Akiba, E. *J. Solid State Chem.* **1995**, *115*, 420.
(18) Kim, J.; Manthiram, A. *J. Electrochem. Soc.* **1998**, *145*, 4, L53.
(19) De Kock, A.; Rossow, M. H.; de Picciotto, L. A.; Thackeray, M. M.; David, W. I. F.; Ibberson, R. M. *Mater. Res. Bull.* **1990**, *25*, 657.
(20) Robertson, A. D.; Bruce, P. G. *Chem. Mater.* **2003**, *15*, 1984.
(21) Kim, J. S.; Johnson, C. S.; Thackeray, M. M. *Electrochem. Commun.* **2002**, *4*, 205.
(22) Tabuchi, M.; Nakashima, A.; Shigemura, H.; Ado, K.; Kobayashi, H.; Sakaebe, H.; Kageyama, H.; Nakamura, T.; Kohzaki, M.; Hirano, A.; Kanno, R. *J. Electrochem. Soc.* **2002**, *149*, A509.
(23) Lubin, F.; Lecerf, A.; Broussely, M.; Labat, J. *J. Power Sources* **1991**, *34*, 161.
(24) Mitzushima, K.; Jones, P. C.; Wiseman, P. J.; Goodenough, J. B. *Mater. Res. Bull.* **1980**, *15*, 783.
(25) Alcantara, R.; Lavela, P.; Tirado, J. L.; Zhecheva, E.; Stoyanova, R. *J. Solid State Electrochem.* **1999**, *3*, 121.
(26) Saadoune, I.; Delmas, C. *J. Solid State Chem.* **1998**, *136*, 8.
(27) Ohzuku, T.; Makimura, Y. *Chem. Lett.* **2001**, *8*, 744.
(28) Lu, Z.; MacNeil, D. D.; Dahn, J. R. *Electrochem. Solid-State Lett.* **2001**, *4*, A191.
(29) Makimura, Y.; Ohzuku, T. *J. Power Sources* **2003**, *119−121*, 156.
(30) Ohzuku, T.; Makimura, Y. *Chem. Lett.* **2001**, *30*, 642.
(31) Yoon, W.; Grey, C. P.; Balasubramanian, M.; Yang, X.; Fisher, D. A.; McBreen, J. *Electrochem. Solid-State Lett.* **2004**, *7*, A53.
(32) Dahn, J. R.; Von Sacken, U.; Michal, C. A. *Solid State Ionics* **1990**, *44*, 87.
(33) Kang, K.; Chen, C.-H.; Hwang, B. J.; Ceder, G. *Chem. Mater.* **2004**, *16*, 2685.
(34) Rieck, H.; Hoppe, R. *Z. Anorg. Alleg. Chem.* **1972**, *392*, 192.
(35) David, W. I. F.; Goodenough, J. B.; Thackeray, M. M.; Thomas, M. G. S. R. *Rev. Chim. Miner.* **1983**, *20*, 636.
(36) Carewska, M.; Scaccia, S.; Croce, F.; Arumugam, S.; Wang, Y.; Greebaum, S. *Solid State Ionics* **1997**, *93*, 227.
(37) Rossouw, M. H.; Thackeray, M. M. *Mater. Res. Bull.* **1991**, *26*, 463.
(38) Johnson, C. S.; Korte, S. D.; Vaughey, J. T.; Thackeray, M. M.; Bofinger, T. E.; Shao-Horn, Y.; Hackney, S. A. *J. Power Sources* **1999**, *81−82*, 491.
(39) Paik, Y.; Grey, C. P.; Johnson, C. S.; Kim, J.-S.; Thackeray, M. M. *Chem. Mater.* **2002**, *14*, 5109.
(40) Pasero, D.; McLaren, V.; de Souza, S.; West, A. R. *Chem. Mater.* **2005**, *17*, 345.

Here we report a nanocrystalline, lithium-rich manganese oxide with a composition very close to Li_2MnO_3 and Mn in the 4+ oxidation state. Detailed structural analyses indicate that the structure of this material is very similar to that of the rock salt monoclinic Li_2MnO_3, with a crystallite size of about 5 nm, and the primary difference appears to be the nanocrystallinity and lack of long-range order in the compound when compared with the microcrystalline Li_2MnO_3. This nanocrystalline Li_2MnO_3-like compound shows lithium intercalation properties that are in dramatic contrast to those of the microcrystalline Li_2MnO_3.

Experimental Section

The nanocrystalline Li_2MnO_3-like compound of this study was synthesized by an aqueous sol−gel method.[41−43] Solid fumaric acid was added to an aqueous solution of lithium permanganate and lithium hydroxide, where the molar ratio of fumaric acid to lithium permanganate used was 1:3. The concentration of lithium permanganate was 0.2 M, and the Li/Mn ratio was controlled at 2:1. After rigorous stirring, gelation occurred in about 10 min and a dark brown, monolithic lithium manganese oxide hydrogel resulted. The hydrogel was frozen using liquid nitrogen and freeze-dried under a vacuum for 24 h using a Flexi-Dry freeze dryer to obtain a lithium manganese oxide cryogel. The cryogel was then heat-treated at different temperatures in air to yield samples with different degrees of crystallinity. In addition to the sol−gel method, a solid-state synthesis method was employed to prepare a crystalline Li_2MnO_3 standard with Li_2CO_3 and $MnCO_3$ as the starting materials. Predetermined amounts of Li_2CO_3 and $MnCO_3$ were carefully mortared together and heated at 500 °C for 72 h and then at 800 °C for 4−8 h to yield a microcrystalline Li_2MnO_3.

X-ray powder diffraction was performed with a Siemens diffractometer using Cu Kα radiation, with a 2θ step size of 0.05° and a dwell time of 10 s at each step. The diffracted beam was monochromatized using a graphite crystal mounted between the sample and the detector. The transmission electron microscopy (TEM) image of the sample was obtained using a Topcon 002B microscope operated at 200 kV. X-ray absorption spectroscopy experiments (XAS) were performed in the PNC-XOR bending magnet beamline (20-BM) of the Advanced Photon Source at the Argonne National Laboratory, IL. Measurements at the Mn K-edge were performed in the transmission mode using gas ionization chambers to monitor the incident and transmitted X-ray intensities. A third ionization chamber was used in conjunction with a manganese standard to provide internal calibration for the alignment of the edge positions. A pair of Si(111) crystals was used to monochromatize the radiation. A rhodium-coated X-ray mirror was utilized to suppress higher-order harmonics. The as-prepared samples and reference standards used for XAS measurements were prepared either as pellets of the active material with boron nitride as the filler or by spreading thin, uniform layers of the powder on Kapton tape and stacking a few layers together to attain the desired absorption step height (typically 0.8−1.0). In situ XAS studies to monitor the electronic and structural changes of the cathode material were performed using a specially designed spectro-electrochemical cell in which the X-ray beam is allowed to pass through the cell, while the discharge−charge cycling is conducted. A detailed construction of the cell is given elsewhere.[44]

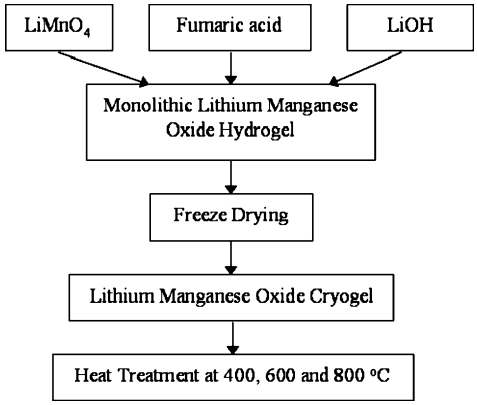

Figure 1. Flowchart of the sol−gel synthesis procedure.

The as-prepared nanocrystalline sample was analyzed for its carbonate content by the test ASTM D513(B), modified for solids. In this analysis, solid powders were titrated with acid to generate carbon dioxide, and the weight of carbonate was determined from the amount of carbon dioxide evolved. This test was performed at a commercial laboratory, Galbraith Laboratories, TN. Electrochemical characterization was carried out with laboratory glass cells. The working electrode mixture was prepared by mixing the active material, carbon powders, and poly(tetrafluoroethylene) (PTFE) binder in a weight ratio ratio of 60:30:10 in a SPEX 8000M mixer mill. The mixture was rolled, punched, and pressed into 1/4 in. diameter pellets with a thickness around 150−200 μm. These pellets were dried under a vacuum at 80 °C for 24 h. Lithium metal foils were used as the counter and reference electrodes, and 1.0 M $LiClO_4$ in 1:1 propylene carbonate/ethylene carbonate (by weight) was used as the electrolyte. The cells were assembled in an argon-circulating glovebox where both moisture and oxygen contents were <2 ppm. The cells thus fabricated were tested at room temperature with a Maccor battery tester.

Results and Discussion

Sol−gel methods are promising alternate routes to solid-state methods for synthesis of a variety of compounds with desired morphology and crystallinity. Products can be obtained at a low temperature via sol−gel routes, allowing synthesis of compounds with amorphous or nanocrystalline structures and nanostructured morphology as well as metastable compositions. Such compounds are difficult to obtain or are often inaccessible by solid-state methods. A flowchart for the synthesis of the nanocrystalline Li_2MnO_3-like compound of this study is given in Figure 1.[42−43] This sol−gel method involves reduction of a permanganate solution using solid fumaric acid, in the presence of a stoichiometric amount of lithium. The lithium-to-manganese ratio is controlled by addition of an appropriate amount of LiOH. The reaction leads to the formation of a monolithic hydrogel. The monolithic hydrogel is then frozen with liquid nitrogen and freeze-dried to remove the water and yield a cryogel. The freeze-drying process limits the surface tension forces typically associated with drying and helps preserve the nanostructured architecture inherent in the parent hydrogel. The starting molar ratio of lithium to manganese, 2:1 in the present study, is precisely preserved through the whole

(41) Bach, S.; Henry, M.; Baffier, N.; Livage, J. *J. Solid State Chem.* **1990**, *88*, 325.
(42) Xu, J. J.; Yang, J. *Electrochem. Commun.* **2003**, *5*, 230.
(43) Yang, J.; Xu, J. J. *J. Power Sources* **2003**, *122*, 181.
(44) Balasubramanian, M.; Sun, X.; Yang, X. Q.; McBreen, J. *J. Power Sources* **2001**, *92*, 1.

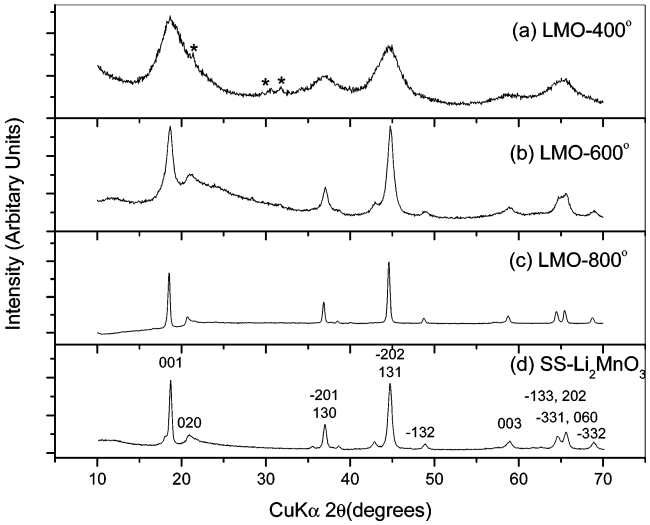

Figure 2. XRD patterns of (a) LMO-400°, (b) LMO-600°, (c) LMO-800°, and (d) SS-Li_2MnO_3. (*) Peaks due to Li_2CO_3. The SS-Li_2MnO_3 pattern (d) is indexed for the *C*2/*m* space group.

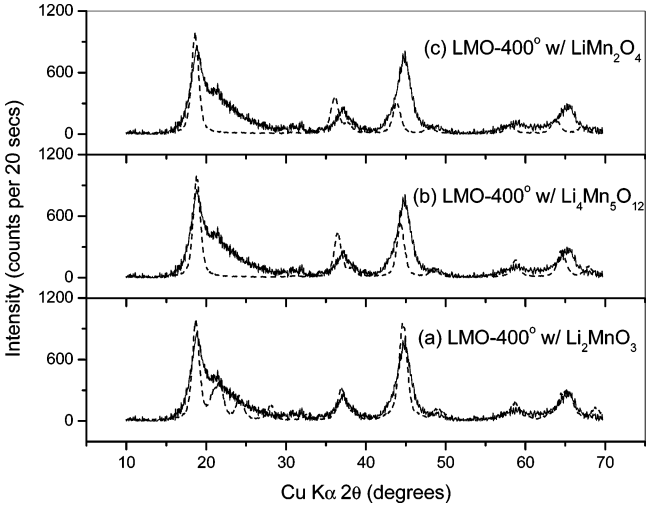

Figure 3. XRD pattern of LMO-400° overlaid with simulated patterns of (a) Li_2MnO_3 (*C*2/*m*, 4.937Å × 8.532 Å × 5.03 Å, $\beta = 109.46°$); (b) $Li_4Mn_5O_{12}$ (*Fd*3*m*, 8.616 Å); and (c) $LiMn_2O_4$ (*Fd*3*m*, 8.247 Å).

synthesis process. The powders obtained after freeze-drying are heat treated for complete reaction of any unreacted components and removal of organic residuals. Different samples were obtained after heat treating the cryogel in air at 400 °C for 24 h, 600 °C for 12 h, and 800 °C for 4 h. These samples are designated as LMO-400°, LMO-600°, and LMO-800°, respectively. Additionally, a Li_2MnO_3 standard has also been synthesized by the solid-state synthesis method as explained in the experimental section, and this sample is designated as SS-Li_2MnO_3.

Figure 2 shows the X-ray diffraction (XRD) spectra of the different samples. A number of compounds in the Li−Mn−O phase diagram, for example, the cubic spinel $LiMn_2O_4$, $Li_4Mn_5O_{12}$, and $Li_2Mn_4O_9$, possess cubic close-packed oxygen framework structures similar to that of Li_2MnO_3, with Mn in the edge-shared octahedral sites. Due to its layered cationic configuration, the Li_2MnO_3 differs from these compounds by lowering of symmetry to a monoclinic structure that can be indexed by a *C*2/*m* space group.[45,46] This lowering of symmetry in Li_2MnO_3 leads to splitting of the (440) peak in the XRD spectrum for the *Fm*3*m* space group of the cubic spinel compounds, such as λ-MnO_2, $Li_4Mn_5O_{12}$, or $Li_2Mn_4O_9$, into the ($\bar{1}$33), (202) and ($\bar{3}$31), (060) twin peaks for the *C*2/*m* Li_2MnO_3,[37] observed at about 63−67°. Also, the Li−Mn ordering in the mixed-cation layer leads to (020), (110), ($\bar{1}$11), and (021) superstructure peaks in the Li_2MnO_3 spectrum between 20 and 30°. The XRD pattern for the LMO-400° sample, Figure 2a, exhibits very broad peaks, clearly indicative of the nanocrystalline structure of the material. The position of these broad peaks and their relative intensities indicate a structure similar to that of Li_2MnO_3. The high-angle tail of the (001) peak and the broad peak structure at 63−67°, likely due to the presence of ($\bar{1}$33), (202) and ($\bar{3}$31), (060) twin peaks, both indicate a strong similarity to the Li_2MnO_3 structure. This is further illustrated by overlaying simulated spectra of the rock salt Li_2MnO_3, spinel $Li_4Mn_5O_{12}$, and $LiMn_2O_4$ phases with the spectrum of LMO-400° (Figure 3). The simulations to obtain spectra for Li_2MnO_3, $Li_4Mn_5O_{12}$, and $LiMn_2O_4$ were conducted using data from the powder diffraction data files for these materials. A commercial powder XRD analysis and simulation software package was used to obtain these spectra. The peak positions and relative peak intensities indicate a strong similarity of the LMO-400° sample to the rock salt monoclinic Li_2MnO_3, while significantly different from the spinel, cubic $Li_4Mn_5O_{12}$ or $LiMn_2O_4$. The broad structure of the LMO-400° peaks, however, does not allow a reasonable whole pattern fitting. Also, due to the weak scattering power of Li ions, disorder in the lithium distribution and the presence of a small amount of other phase(s) cannot be completely ruled out from the XRD analysis.

The broad peaks of the LMO-400° sample evolve into the enhanced peaks of the LMO-600° and LMO-800° samples, Figure 2b,c, as the heat treatment temperature is increased. The XRD pattern of the LMO-600° sample, Figure 2b, shows well-discernible peaks that are characteristic to the Li_2MnO_3; however, the breadth of these peaks indicate the weaker crystallinity/smaller crystallite size of this sample than of microcrystalline Li_2MnO_3. The XRD pattern of the LMO-800° sample (Figure 2c) shows fully developed sharp peaks and can be indexed to Li_2MnO_3 with a monoclinic rock salt structure with a *C*2/*m* space group with lattice parameters of 4.915 × 8.533 × 5.016 Å and $\beta = 109.203°$. Figure 2d shows the XRD spectrum of the SS-Li_2MnO_3 sample. This sample can be indexed to Li_2MnO_3 with a *C*2/*m* space group and lattice parameters of 4.923 × 8.559 × 5.022 Å and $\beta =$ 109.316°. This sample appears to have a slightly weaker crystallinity than the sol−gel LMO-800° sample. The LMO-800° and the SS-Li_2MnO_3 samples both do not show well-developed superstructure peaks at 20−30° but a waning tail after the (001) peak, indicating only weak lithium and manganese ordering in the mixed-cation layers.

In the spectrum for the LMO-400° sample additional peaks that cannot be attributed to a Li_2MnO_3 structure are also seen, as marked in Figure 2a. Careful analyses of these peaks reveal that these correspond to the phase Li_2CO_3, indicating

(45) Strobel, P.; Lambert-Andron, B. *J. Solid State Chem.* **1988**, *75*, 1, 90.
(46) Massarotti, V.; Bini, M.; Capsoni, D.; Altomare, A.; Moliterni, A. G. G. *J. Appl. Crystallogr.* **1997**, *30*, 123.

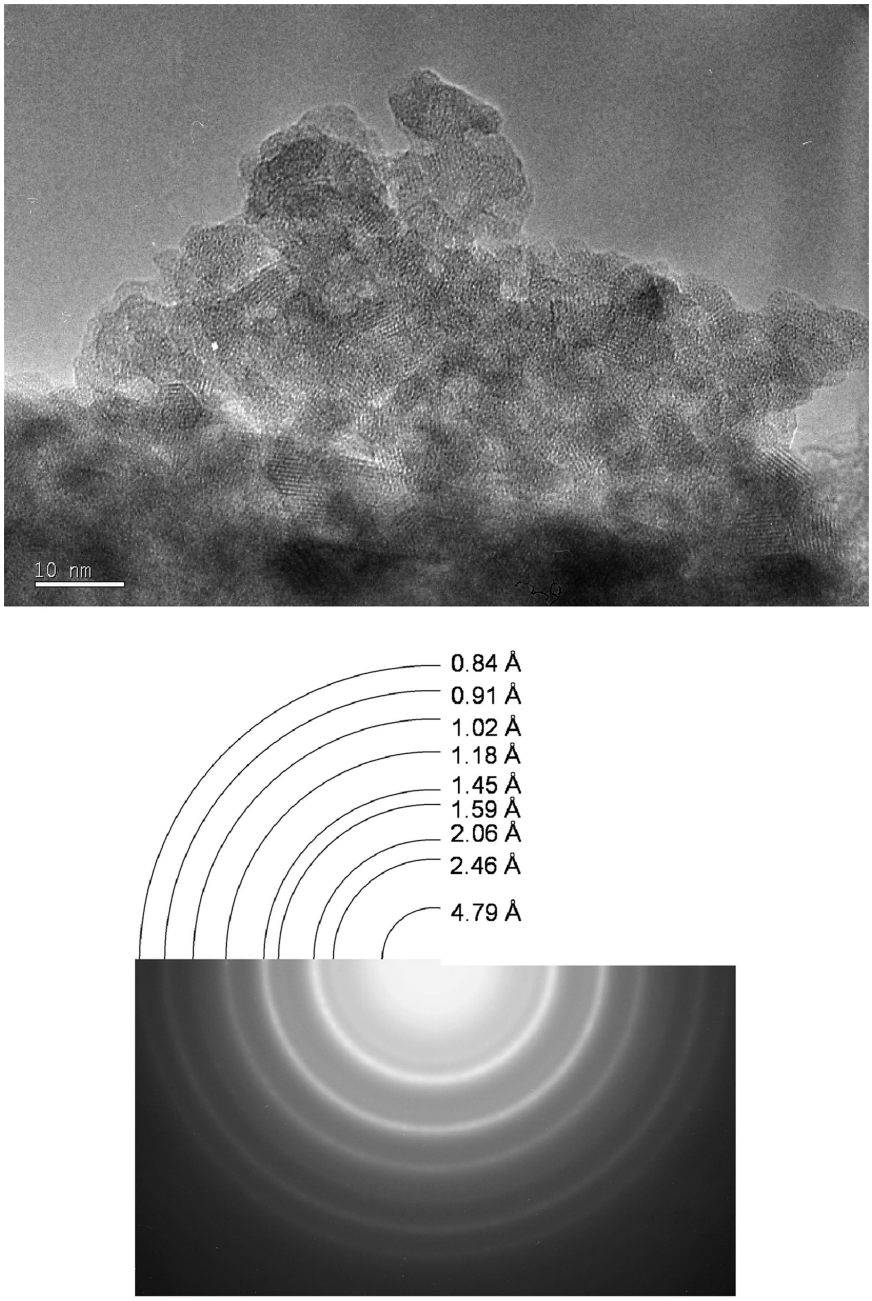

Figure 4. HRTEM image and SAED pattern of LMO-400°.

that a small fraction of the lithium added to the system remains unreacted with manganese oxide after heat treatment at 400 °C and forms the phase Li_2CO_3. The LMO-600° sample and LMO-800° sample do not show peaks due to any impurity Li_2CO_3 phase. A determination of the amount of Li_2CO_3 present was done by an ASTM method for analysis of carbonates in solids, as explained in the experimental section. This test indicates that the LMO-400° sample contains 2.8 wt % of Li_2CO_3, while the bulk of the material is Li_2MnO_3 with a small overall lithium deficiency. The amount of lithium trapped in 2.8 wt % of Li_2CO_3 corresponds to a lack of 0.08 Li per Li_2MnO_3.

Figure 4 shows a high-resolution transmission electron microscopy (HRTEM) image and selected area electron diffraction (SAED) pattern of LMO-400°, both of which clearly illustrate the nanocrystalline structure of the sample. The image in Figure 4 shows crystallites of about 5 nm in size, with evident lattice fringes indicating good crystallinity. There are no apparent amorphous regions in the TEM image, although there must be some disordered interfacial areas between these nanosized crystallites. Interplanar spacing was measured from the lattice fringes in the HRTEM image, and an average value of 4.8 Å was obtained, which corresponds to the (001) plane of the monoclinic, rock salt Li_2MnO_3 structure. The electron diffraction pattern in Figure 4 was obtained from approximately a 200 nm × 200 nm area of the sample. The ring pattern has been indexed using the software developed by Labar.[47] The rings yield lattice spacings which rather precisely correspond to the interplanar spacings of the strongly diffracting sets of planes of the monoclinic, rock salt Li_2MnO_3 structure. Also, the size of the crystallites seen in the TEM image, about 5 nm, is in

(47) Lábár, J. L. *Microscopy and Analysis* **2002**, *75*, 9.

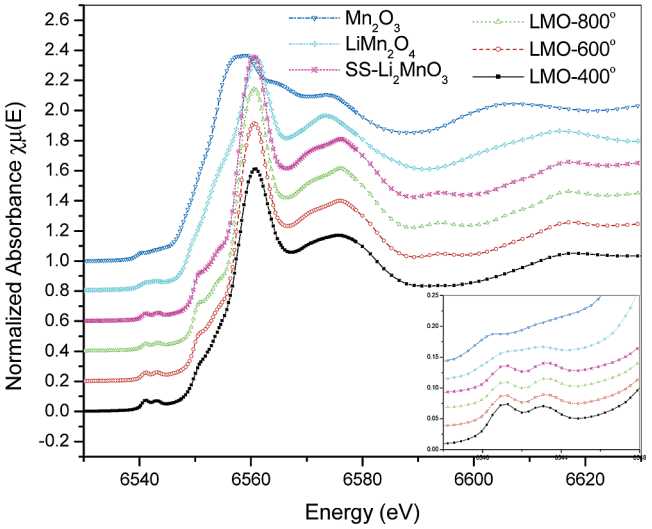

Figure 5. XANES spectra of the Mn_2O_3 standard, the $LiMn_2O_4$ standard, the SS-Li_2MnO_3 sample, and LMO-800°, LMO-600°, and LMO-400° samples (from top to bottom). Inset shows the expanded pre-edge region. The curves are offset in the *y* direction for clarity.

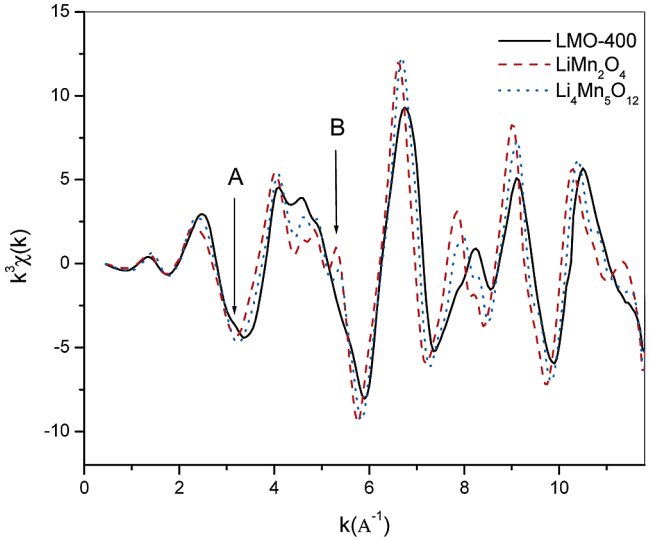

Figure 6. EXAFS $k^3\chi(k)$ spectra of LMO-400° compared to that of the spinel $LiMn_2O_4$ and $Li_4Mn_5O_{12}$ standards. Arrows A and B mark the features which are dissimilar in the sample and the standards.

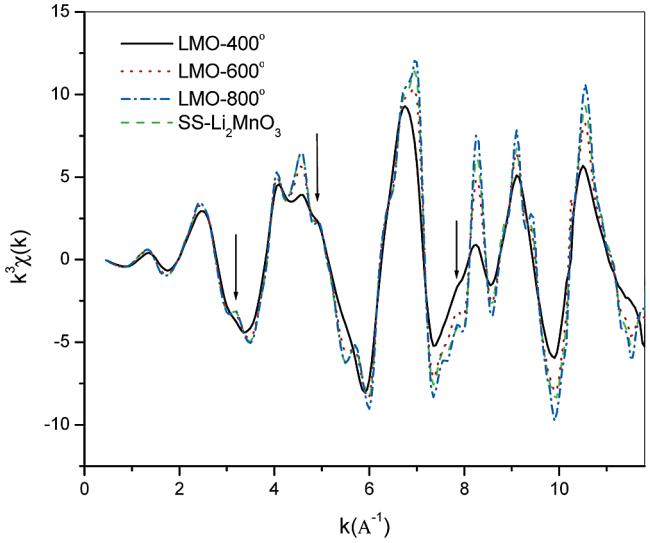

Figure 7. EXAFS $k^3\chi(k)$ spectra of LMO-400° compared to those of LMO-600°, LMO-800°, and SS-Li_2MnO_3. Arrows mark the features in the crystalline samples that are also observed in the nanocrsytalline LMO-400°, albeit diminished in intensity.

excellent agreement with that estimated from the broadening of the XRD peaks (Figure 2a) via the Scherrers equation, which also comes out to be about 5 nm.

XAS measurements were conducted at the Mn K edge for the LMO-400°, LMO-600°, LMO-800°, and SS-Li_2MnO_3 samples. XAS measurements were also conducted on a few manganese oxide standards such as Mn_2O_3, $LiMn_2O_4$, and $Li_4Mn_5O_{12}$. To determine the formal oxidation state and investigate the local structure of the various samples, we first compare the Mn K-edge X-ray absorption near-edge structure (XANES) of various samples to the spectra of various Mn-containing oxides as standards. Figure 5 shows the Mn XANES of LMO-400°, LMO-600°, and LMO-800° compared to the spectra of Mn_2O_3, $LiMn_2O_4$, and SS-Li_2MnO_3. It is clearly evident that the edge position of the samples generated by the sol−gel method, namely, LMO-400°, LMO-600°, and LMO-800°, is coincident with that of SS-Li_2MnO_3 but is shifted significantly to higher energies when compared to the Mn_2O_3 (Mn^{3+}) and $LiMn_2O_4$ ($Mn^{3.5+}$) standards. The pre-edge region (shown expanded in the inset) also shows a similar trend. These observations confirm that the oxidation state of Mn in LMO-400°, LMO-600°, and LMO-800° is 4+, similar to that expected for SS-Li_2MnO_3. While the edge position depends on the oxidation state, the shape of the near-edge spectra also depends on the local- and medium-range (∼5−10 Å) atomic structure. The close similarity of the near-edge specta of LMO-400°, LMO-600°, LMO-800°, and SS-Li_2MnO_3 indicates that the local structure is similar in these samples. The only slightly different shape of the near edge of the LMO-400° sample is probably related to the less crystalline nature of this sample and effects due to slight lithium nonstoichiometry in the compound.

Extended X-ray absorption fine structure spectroscopy (EXAFS) data of the LMO-400° sample and the spinel $LiMn_2O_4$ and $Li_4Mn_5O_{12}$ standards are presented in Figure 6. This comparative analysis of the local structure of the LMO-400° sample to these compounds is helpful for fully establishing that the structure of the compound is similar to that of the rock salt monoclinic Li_2MnO_3 and not to the spinel phases that are electrochemically active. Close inspection of the complex beat pattern in the 2−6 $Å^{-1}$ region reveals significant difference between the LMO-400° sample and the $LiMn_2O_4$ and $Li_4Mn_5O_{12}$ spinels. In particular, feature A present as a shoulder in LMO-400° is absent in the spinels. At the same time, feature B present in the spinels is absent in the LMO-400°. These observations clearly show that the medium-range local structure of the LMO-400° sample is different from that of the spinels. Next we compare the EXAFS spectra of the LMO-400°, LMO-600°, and LMO-800° samples with that of the SS-Li_2MnO_3 sample (Figure 7). The spectra of LMO-400°, LMO-600°, and LMO-800° are similar to that of SS-Li_2MnO_3. The similarity in the complex beat pattern of LMO-400°, LMO-600°, and LMO-800° to that of SS-Li_2MnO_3 clearly indicates that the medium-range structure around Mn in the sol−gel samples is similar to that around Mn in SS-Li_2MnO_3. However, high-frequency components, which appear as well-defined features

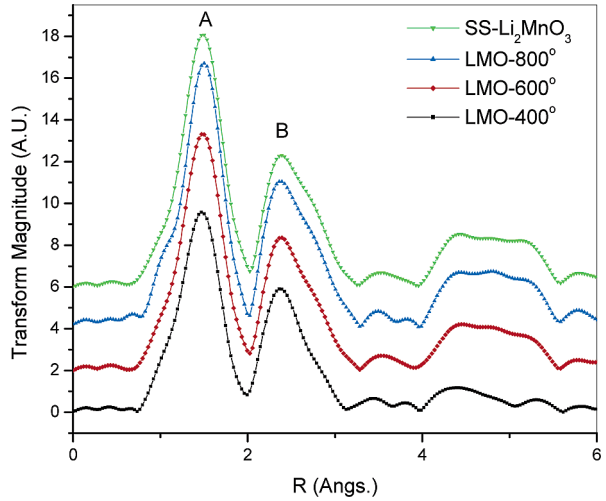

Figure 8. Pseudo-RDF patterns of SS-Li_2MnO_3, LMO-800°, LMO-600°, and LMO-400° (from top to bottom). (A) Mn−O correlation, (B) Mn−Mn correlation. The curves are offset in the *y* direction for clarity.

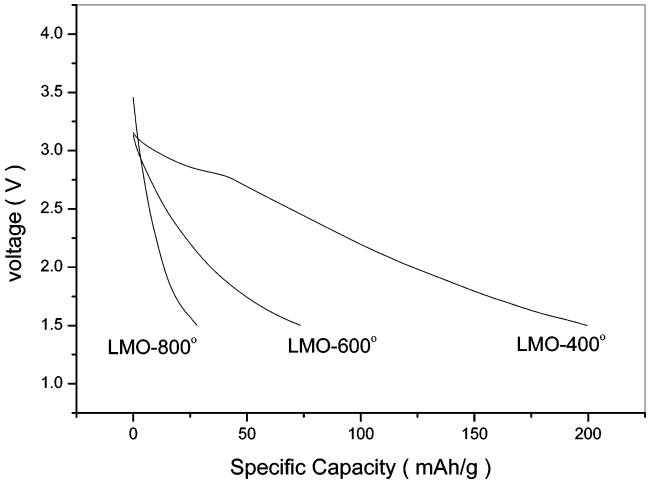

Figure 9. First discharge profiles of LMO-400°, LMO-600°, and LMO-800° at a rate of 50 μA/cm^2 or C/100.

in SS-Li_2MnO_3, such as the ones indicated by arrows, appear as shoulders in the LMO-400° sample. High-frequency components arise from scattering (of the photoelectron) processes that involve long scattering paths; that is, scattering by distant neighbors and multiple-scattering processes. The diminished intensity of the features for the LMO-400° sample is due to its less crystalline and more disordered nature. The intensity of the high-frequency features systematically increases on heat treatment, in agreement with the increased crystallinity of the LMO-600° and LMO-800° samples.

Figure 8 shows the Fourier transform (FT) magnitude of the EXAFS signal of the LMO-400°, LMO-600°, and LMO-800° samples compared with that of SS-Li_2MnO_3. The first peak (labeled A) arises from Mn−O correlations. The second peak (labeled B) arises from Mn−Mn correlations. The position of these peaks and their general appearance are very similar for all samples. These observations strongly suggest that the local environment of Mn is similar in all samples. The lower magnitude of the peak heights for LMO-400° is consistent with the less crystalline nature of this sample. The FTs of LMO-600°, LMO-800°, and SS-Li_2MnO_3 also exhibit peaks in the 4−6 Å range, while distinct peaks are not evident for the LMO-400° sample. These peaks arise from longer-range correlations and multiple scattering paths and reflect the more crystalline nature of the LMO-600°, LMO-800°, and SS-Li_2MnO_3 samples when compared to the LMO-400° sample.

Structural analysis of the as-prepared materials by XRD and XAS, along with HRTEM and SAED of LMO-400°, has established that the structures of the LMO-400°, LMO-600°, and LMO-800° samples are very similar to that of the rock salt monoclinic Li_2MnO_3. The primary difference between the LMO-400° sample and the LMO-800° or SS-Li_2MnO_3 samples is just the lack of long-range order in the former, namely, nanosized crystallites in the former versus microcrystalline structure of the latter, while the crystallinity of the LMO-600° sample falls between. However, electrochemical tests have revealed that the former is electrochemically highly active and capable of reversibly intercalating large amounts of lithium ions, while the latter is electrochemically inactive. Electrochemical properties of the different samples were measured under the galvanostatic mode. Figure 9 shows the discharge profiles of different samples from the open circuit voltage to 1.5 V versus Li^+/Li at a current density of 50 μA/cm^2. This current rate roughly corresponds to a slow discharge rate of C/100, that is, intercalation of 1 mol of Li per Li_2MnO_3 per 100 h. These tests are indicative of the intrinsic intercalation capacities of these materials, since kinetic limitations are minimized at such a slow rate. In these tests, the fully crystalline LMO-800° sample yields a specific capacity of merely 28 (mA h)/g. The discharge profile of this microcrystalline sample shows sloping voltages, with no particular features in the profile. This performance of the LMO-800° sample is consistent with that reported in the literature[5,20−23] and shows that the microcrystalline Li_2MnO_3 compound is indeed electrochemically inactive for lithium intercalation or discharge, at least down to 1.5 V versus Li^+/Li. Under the same test conditions, the LMO-600° sample yields a specific capacity of 75 (mA h)/g, corresponding to intercalation of 0.32 Li per Mn, substantially higher than that of the crystalline LMO-800° sample. Furthermore, the LMO-400° sample shows a specific capacity of 200 (mA h)/g, corresponding to intercalation of 0.87 Li per Mn, dramatically higher than the microcrystalline LMO-800° sample. The corresponding specific energy delivered is 446 (mW h)/g, which is promising in comparison to the about 500 (mW h)/g delivered by the state-of-the-art $LiCoO_2$. The high intercalation capacity of the LMO-400° sample illustrates how an electrochemically inactive Li_2MnO_3 can be turned highly active when the long-range crystal structure order is reduced to the range of a few nanometers. Considering the intermediate capacity of the LMO-600° sample, the data show a trend toward higher intercalation capacities with samples whose crystal structure order extends to shorter length scales.

Next, the samples were discharged and charged repeatedly at a higher current value of 1 mA/cm^2, roughly corresponding to a C/5 rate. Figure 10 shows the discharge and charge profiles for the first and the second cycles (the second cycle plot is displaced by 75 (mA h)/g for clarity). The LMO-400° sample shows a discharge capacity of 163 (mA h)/g or

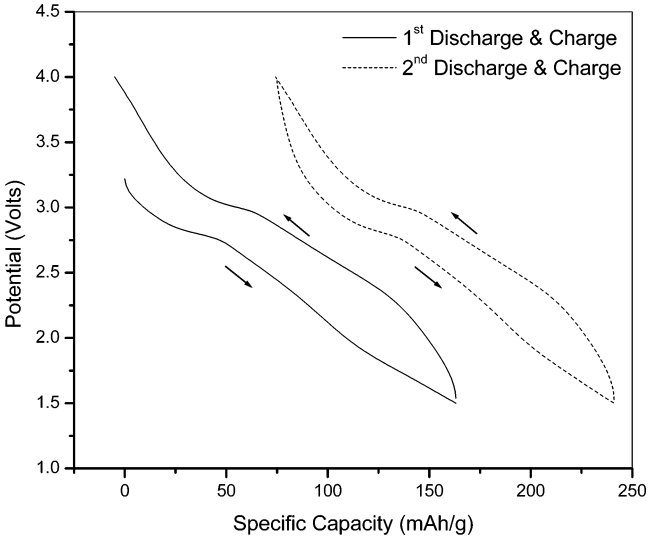

Figure 10. Discharge and charge profiles for the first and second cycles for LMO-400° at a rate of 1 mA/cm^2 or C/5. The profiles for the second cycle are offset by 75 (mA h)/g for clarity.

0.71 Li/Mn for the first discharge and nearly perfect reversibility upon charging. The figure illustrates the excellent reversibility of the compound, seen not only in terms of the values of discharge and charge capacities, but also the very low hysteresis between the discharge and charge steps. The features seen in the initial discharge/charge cycles are repeated during subsequent cycles. Data for the 50th cycle, not shown here, still show low hysteresis and excellent charge/discharge reversibility, albeit with a lower capacity of 151 (mA h)/g. The discharge profile of the LMO-400° sample shows a relatively flat region around 2.8 V and a sloping voltage curve thereafter. The discharge feature in the region around 2.8 V appears similar to the 2.8 V plateau observed in different cubic-spinel compounds for intercalation in octahedral sites. The possibility of intercalated lithium occupying a small amount of vacant octahedral sites in LMO-400° is discussed below. The sloping voltage profile beyond the 2.8 V region suggests that the Li intercalation is associated with sites with varying intercalation potential. Such a sloping voltage profile is a strong characteristic of nanostructured materials and may be associated with dispersion in site potentials due to weak long-range crystallinity in such materials.

Figure 11a shows the cycling performance of the three samples at a C/5 discharge/charge rate. The LMO-400° sample shows an initial specific capacity of 163 (mA h)/g and delivers a rather stable capacity over repeated cycling. The capacity retention upon repeated cycling for the LMO-400° sample is promising in comparison to other manganese oxide based cathode candidates. As discussed before, the lithium-rich composition of the material and the 4+ oxidation state of Mn likely provide improved structural as well as chemical stability to the compound. The nanostructured morphology and the lack of a long-range-order structure in the compound may also contribute toward attaining this superior reversibility, as has been reported in a number of cases before.[49−51] Figure 11b shows the charge coefficient data (the ratio of charge capacity to discharge capacity) for the LMO-400° sample, corresponding to the cycling data presented in Figure 11a. The charge coefficient value constantly stays very close to 1, indicating that the amount of lithium extracted or deintercalated is the same as the amount intercalated, and that the lithium ions present in the starting compound are not participants in the intercalation/deintercalation process. This value of the charge coefficient also indicates the lack of any non-Faradaic parasitic reactions in the system.

In contrast with LMO-400°, the LMO-600° and LMO-800° samples show capacities of about 50 (mA h)/g and 25 (mA h)/g, respectively. Notably, the LMO-800° sample delivers a capacity of 28 (mA h)/g at C/100 and 25 (mA h)/g at C/5. This negligible difference in capacity at these vastly different rates shows that the insignificant capacity of LMO-800° is not due to kinetic limitations, since discharge at a much lower rate does not result in higher capacity. It emerges that the LMO-800° sample is inherently unable to allow lithium intercalation, as has been reported in previous studies on the microcrystalline rock salt Li_2MnO_3.[5,20−23] The LMO-400° material, on the other hand, shows a capacity of 200 (mA h)/g at C/100 and 163 (mA h)/g at C/5, indicating the effect of kinetics on the attainable capacity during discharge.

Next we present in situ XANES data obtained for the LMO-400° sample. XAS scans were collected continuously during discharge of the sample at a rate close to C/10. The discharge capacity obtained was about 191 (mA h)/g, equivalent to intercalation of 0.83 Li per Mn. Figure 12a shows the XANES plot for the 1st, 5th, 10th, 15th, 20th, and 25th scans, representing roughly 0, 20, 40, 60, 80, and 100% depths of discharge, respectively. The data show a continuous, systematic lowering of the edge position along with the discharge, signifying a clear decrease in the Mn oxidation state. The edge shows a rigid movement during discharge, with a total decrease in the edge energy of about 2.1 eV. This must correspond to the change in Mn oxidation state during discharge from 4+ to about 3.17+, as indicated by the electrochemical data. The XANES spectrum for the fully discharged state, in Figure 12a, shows an absorption edge position significantly lower than that of $LiMn_2O_4$ ($Mn^{3.5+}$) but closer to that of Mn_2O_3 (Mn^{3+}), in agreement with the expected average oxidation state of 3.17+. These data clearly show a Faradaic decrease in the Mn oxidation state during discharge and show no evidence of any significant amount of non-Faradaic processes occurring in the cell.

Inspection of the XANES data during discharge also reveals the absence of isosbestic points; that is, the spectra taken at various states of discharge do not exhibit a common set of intersection points. If the material were to undergo a two-phase reaction, the corresponding in situ spectra would exhibit a single set of isosbestic points, as reported in studies

(48) Kang, S. H.; Goodenough, J. B.; Rabenberg, L. K. *Electrochem. Solid-State Lett.* **2001**, *4*, A49.
(49) Jang, Y. I.; Huang, B.; Wang, H.; Sadoway, D. R.; Chiang, Y. M. *J. Electrochem. Soc.* **1999**, *146*, 3217.
(50) Xu, J. J.; Jain, G. *Electrochem. Solid-State Lett.* **2003**, *6*, A190.
(51) Jain, G.; Charles, C. J.; Xu, J. J. *J. Electrochem. Soc.* **2003**, *150*, A806.

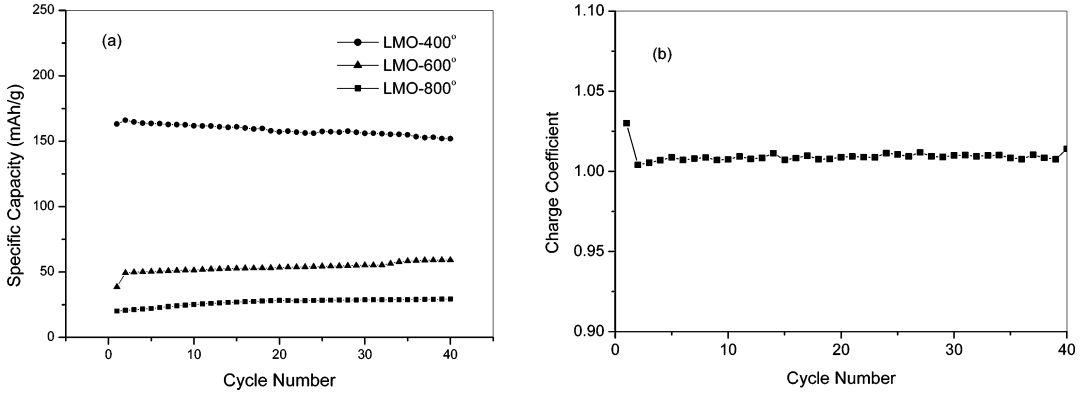

Figure 11. (a) Cycling performance of LMO-400°, LMO-600°, and LMO-800° at 1 mA/cm^2 or C/5; (b) charge coefficient (charge capacity/discharge capacity) data for LMO-400°.

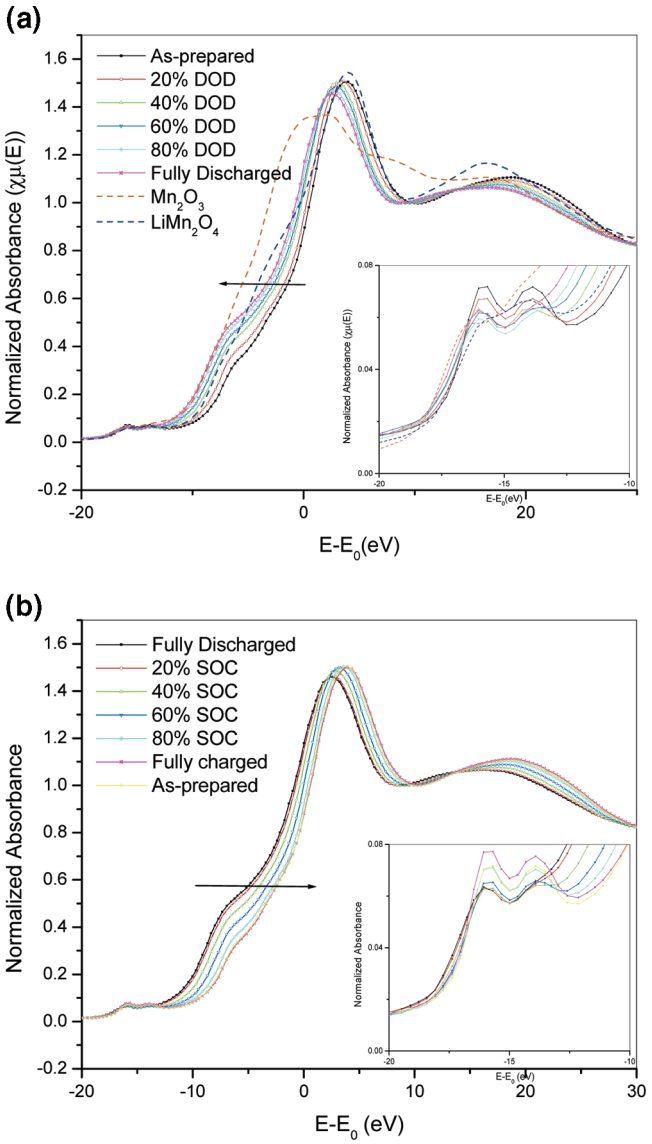

Figure 12. XANES spectra of LMO-400° at various depths of discharge (a) and charge (b). Inset shows the respective expanded pre-edge region. In part a, the spectra for reference compounds Mn_2O_3 and $LiMn_2O_4$ are provided for comparison.

on other systems.[52,53] The absence of isosbestic points suggests the occurrence of a single phase topotactic reaction or the formation of intermediates whose structure changes continuously. During a single-phase topotactic reaction, the structure of the compound evolves continuously as the discharge progresses leading to the absence of isosbestic points. This inference regarding the absence of a two-phase reaction is consistent with the highly sloping electrochemical discharge profile of this material.

The XANES spectra collected on the same sample during the first charge (following the first discharge) are shown in Figure 12b. The spectra show an increase in the edge energy with successive charging scans, signifying an increase in the Mn oxidation state and occurrence of Faradaic charging in the sample. Notably, the spectrum for the fully charged state coincides perfectly with the spectrum for the as-prepared material (Figure 12b), indicating excellent structural reversibility during the first discharge/charge cycle. These data demonstrate the Faradaic discharge and charge processes occurring in the LMO-400° sample, strongly suggesting that a highly reversible lithium intercalation reaction is indeed the predominant mechanism behind the electrochemical behavior of the sample.

A striking observation from these in situ data is the evidence of perfect reversibility of the local structure of the nanocrystalline LMO-400° sample during the first cycle. The EXAFS data (not shown here) also illustrate the perfect structural reversibility of the material during the first cycle. To further investigate the structural stability of the compound, we have conducted XRD on the LMO-400° cathode pellets after electrochemical tests. For these XRD tests, pellets were washed in the solvent propylene carbonate/1,2-dimethoxyethane (in 1:1 ratio by weight) for 24−48 h and dried for 24 h under vacuum before conducting the XRD. Figure 13 shows the XRD pattern of the as-prepared LMO-400° sample (a), after first discharge (b) and after 25 discharge/charge cycles (c). The spectrum of the sample after the first discharge does not show evidence of formation of any new phase or occurrence of any structural changes, in agreement with the in situ XAS data. Furthermore, the XRD of the charged sample after 25 cycles is nearly identical to that of the as-prepared material, indicating the exceptional reversibility of the compound upon repeated lithium intercalation/deintercalation cycling. This unusual stability and reversibility of the nanocrystalline compound may be especially appreciated considering that microcrystalline lithium man-

(52) Wang, X.; Hanson, J. C.; Frenkel, A. I.; Kim, J.-J.; Rodriguez, J. A. *J. Phys. Chem. B* **2004**, *108*, 13667.
(53) Jain, G.; Balasubramanian, M.; Xu, J. J. *Chem. Mater.* To be submitted.

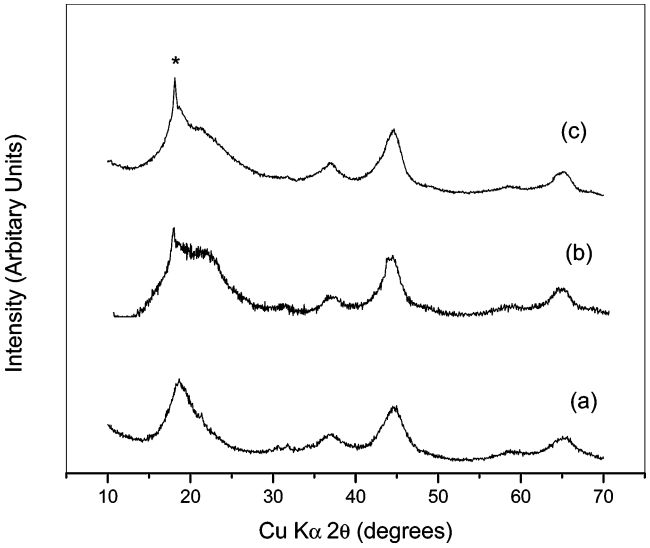

Figure 13. XRD patterns of the as-prepared LMO-400° sample (a), after first discharge (b), and after 25 discharge/charge cycles (c). The sharp peak (ca. 18°) in spectra b and c is due to PTFE binder.

ganese oxide compounds, for example, the well-known spinel $LiMn_2O_4$, encounter problems of structural instability and irreversibility caused by the Jahn−Teller effect involving Mn^{3+} during lithium intercalation and that the nanocrystalline compound here clearly involves a high percentage of Mn^{3+} as well during the intercalation process as evidenced by both the electrochemical data and the XANES analysis.

Even more striking is consideration of the fact that stoichiometric, microcrystalline Li_2MnO_3 does not allow intercalation of lithium, due to the unavailability of octahedral sites. Stoichiometric rock salt compounds are generally considered the end composition for intercalation. As explained in the introduction, efforts to insert lithium into rock salt compounds have resulted in either precipitation of Li_2O and the transition metal[32] or occurrence of a phase transformation entailing migration of some of the cations from the octahedral to the tetrahedral sites.[5,32,35] Yet large amounts of lithium are reversibly intercalated into the nanocrystalline Li_2MnO_3-like compound, LMO-400°, in this study. As seen via our post-discharge XRD data and lack of isosbestic points in the in situ XANES data, a simple phase transformation involving the coexistence of two Mn-containing phases most likely does not occur in the nanocrystalline LMO-400° sample. We believe that the slight nonstoichiometry in the compound may be partly responsible for the observed intercalation capacity. Lithium intercalation has been reported in samples obtained upon acid leaching of Li_2O from Li_2MnO_3 samples.[37−39] Similar to these samples, the nonstoichiometry in the Li content by 0.08 Li per Li_2MnO_3 in the LMO-400° sample, caused due to the presence of the impurity phase Li_2CO_3, must allow accommodation of a small amount of Li in vacant octahedral sites. The possibility of somewhat different distribution of lithium in the more disordered as-prepared material as compared with that in the microcrystalline counterpart, one that could not be completely ruled out by the X-ray analysis, might give rise to more vacant octahedral sites. As discussed before, the discharge curve for the LMO-400° sample, in Figures 9 and 10, shows part of the discharge capacity associated with a relatively flat and small voltage region around 2.8 V, which may correspond to intercalation in octahedral sites. The bulk of the intercalation capacity of 0.87 Li per Mn, however, cannot be attributed to accommodation into vacant octahedral sites. The nanostructured particles with their disordered surface structure may allow accommodation of a significant amount of Li into noncrystallographic surface sites. Such intercalation/deintercalation is expected to be facile, show a sloping voltage profile, and allow good reversibility, in agreement with the observed data. However, such sites would still be unlikely to account for all of the 0.87 Li per Mn capacity. It is evident from the HRTEM image (Figure 4) that there are no large amorphous or disordered regions. Other possibilities, perhaps most provocatively the possibility of occupation of interstitial sites by lithium in the structure of a nanocrystalline or nanostructured rock salt compound, need to be explored. In microcrystalline rock salt compounds, such occupation would be energetically too unfavorable to occur and a phase transformation would be unavoidable upon such insertion. However, the energetics of intercalation in nanocrystalline or nanostructured compounds can be significantly different from that in their microcrystalline counterparts.[50,53] The disordered structure of the nanocrystalline compound beyond the short range, as evidenced by the EXAFS $k^3\chi(k)$ spectrum and the pseudo-RDF pattern in comparison with that of the microcrystalline counterparts (Figures 7, 8), might also make insertion of lithium ions into the interstitial sites of the compound more feasible. Furthermore, nanostructured morphology could help accommodate volume changes and stress and strain introduced in the grains or particles during lithium intercalation/deintercalation and alter the overall energetics to alleviate or suppress the tendency for a phase transformation.[48,49] The nanocrystalline structure and nanostructured morphology of the current material makes structural characterization and a direct determination of sites occupied by lithium a rather difficult task. The weak scattering power of lithium for X-rays, along with the lack of long-range-order crystal structure, renders determination of lithium intercalation sites via X-ray methods infeasible. Experiments based on solid-state NMR or neutron diffraction would be better able to bear on investigation of the specific sites occupied by lithium in the nanocrystalline compound and will be pursued in future studies. The results of the present study highlight the qualitative difference in the intercalation behavior of nanocrystalline, rock salt Li_2MnO_3 and its microcrystalline counterpart and point to the fact that nanostructured intercalation compounds may exhibit unusual and surprising properties in dramatic contrast with conventional microcrystalline compounds. In addition to fundamental scientific interest, exploration of such properties could also lead to technological applications. Technological implications of the findings of the present study and their possible extension to other rock salt compounds may be appreciated in light of the prominent role of rock salt compounds in rechargeable lithium battery technology.

Conclusion

A nanocrystalline Li_2MnO_3 compound with a crystallite size of about 5 nm is reported as a surprising lithium

intercalation host. XRD, HRTEM, SAED, and XAS analyses establish the structural similarity of the compound to the rock salt monoclinic Li_2MnO_3. Electrochemical tests illustrate the ability of the nanocrystalline compound to allow large-capacity, reversible lithium intercalation with excellent cycling performance, in sharp contrast to the microcrystalline rock salt Li_2MnO_3, which has been known to be electrochemically inactive and incapable of intercalating any significant amount of lithium. In situ XAS experiments demonstrate Faradaic Mn reduction/oxidation processes occurring in the material during discharge/charge. XAS and XRD analyses also reveal exceptional structural stability and reversibility of the material during lithium intercalation and repeated discharge/charge cycling. The study points toward novel phenomena and unusual properties associated with nanocrystalline or nanostructured intercalation compounds and highlight the possibility of a qualitative difference in intercalation behavior compared with their microcrystalline counterparts.

Acknowledgment. The authors thank Dr. James McBreen and Dr. Won-sub Yoon (Brookhaven National Laboratory) for their help with initial XAS study. The authors would also like to thank Dr. Daniel Abraham (CMT, Argonne National Laboratory) for help with electrochemical testing at ANL and Dr. Jafar Al-Sharab (Rutgers University) for help with TEM experiments. This work is supported by the NSF Industry/University Collaborative Research Program on Ceramic and Composite Materials at Rutgers University/Penn State University/University of New Mexico. Partial support of the Office of Naval Research is gratefully acknowledged. PNC-CAT facilities at the Advanced Photon Source and research at these facilities are supported by the US DOE Office of Science Grant DEFG03-97ER45628, the University of Washington, a major facilities access grant from NSERC, Simon Fraser University, and the Advanced Photon Source. Use of the Advanced Photon Source is also supported by the U.S. Department of Energy, Office of Science, Office of Basic Energy Sciences, under Contract No. W-31-109-Eng-38.

CM0503329